# Detection of Structural Defects in Pipes using Time Reversal of Guided Waves

Nicholas O'Donoughue, Joel Harley, José M.F. Moura
Electrical and Computer Engineering
Carnegie Mellon University
Pittsburgh, PA 15213

Yuanwei Jin
Engineering and Aviation Sciences
Univ. of Maryland, Eastern Shore
Princess Anne, MD 21853

***Abstract*—Structural health monitoring of buried pipelines is of vital importance as infrastructures age. Ultrasonic guided waves are a popular method for inspecting buried pipes, due to their potential for long propagation. Unfortunately, the large number of wave modes present, and the effects of dispersion, in a pipeline make analysis of the received signals difficult. We plan to use Time Reversal Acoustics to compensate for these complex signals, and improve performance for the detection of faults in a pipeline. We will present theoretical performance results for conventional and Time Reversal detectors, verified with simulations conducted in PZFlex. Time Reversal shows a potential for a reduction in the power requirements of a fault detection system.**

***Index Terms*—Time Reversal, structural health monitoring, dispersion, buried pipelines, PZFlex**

## I. Introduction

Buried pipelines are an integral part of any country's infrastructure, as they are commonly used to transport liquids and gases, such as crude oil and natural gas, from their excavation sites to processing facilities, and to the consumers. In the United States alone, there were 180 natural gas pipeline accidents in 2008. These accidents accounted for 7 fatalities, 66 injuries, and $302,268,941 in property damage [1]. Consequently, it is of vital importance that these buried pipelines be inspected and certified to be free of damage. Many current solutions utilize guided waves [2], [3] due to their long propagation distances. However, dispersion and mode-dependent group speeds make interpretation of wideband signals difficult [4]. In order to alleviate these problems, large rings of transducers are used to selectively excite a single wave mode, and a narrow bandwidth is used to limit dispersive effects. This results in large power requirements, and a relatively short probing distance from the transducer array. We will alleviate these restrictions by exploiting the benefits of Time Reversal, a signal processing technique first pioneered in acoustics by M. Fink [5].

The use of guided waves for non-destructive testing in pipes is complicated by the propagation environment. When a thin plate is excited by acoustic pressure waves, it responds with a countably-infinite number of discrete guided waves. These waves all travel with independent velocities, and experience an effect termed frequency dispersion. We consider here a hollow pipe, which has the added complexity of multiple independent paths that can be taken by each wave around the pipe as they progress. All of these factors complicate the system's response to input, and make conventional processing more difficult. Many of the wave modes can be suppressed by utilizing relatively small frequency bands, and by intelligently designing the excitation transducer array, and the effects of frequency dispersion can be similarly limited. But these approaches unnecessarily restrict the design of inspection systems.

Time Reversal has been shown to compensate for both dispersiveness and the multi-modal environments found in thin plates, where lamb waves exist [6], [7], and in hollow pipes, where guided waves exist [8], resulting in a compression of the wave in both time and space and an increase in the peak signal level. From [9], [10], we know that Time Reversal's focusing effects are most visibly seen in extremely dense channels, with discrete echoes generated from scattering objects. In this paper, we apply detection algorithms derived for Time Reversal arrays [10] to the hollow pipe scenario under consideration. We show that in both the ideal case (with the channel response known fully) and the realistic case (where it must be estimated), time reversal processing achieves a notable increase in detection performance. We note that, while many systems operate in a pulse-echo mode, we are devising this system for a pitch-catch scenario, and make the comparison in this paper between only pitch-catch scenarios.

The remainder of the paper is organized as follows. Section II describes our physical model. Section III lays out the transmission scheme and detectors used, while the reader is referred to [10] for a detailed derivation. We describe the numerical simulations performed in Section IV, and provide our conclusions in Section V.

## II. Physical Model

In this paper, we consider a hollow pipe, with thin walls relative to its length and diameter. The thin walled assumption allows us to consider guided wave propagation. Guided waves in hollow cylinders fall into three general categories: torsional, longitudinal, and flexural [4]. The torsional modes induce particle motion in the circumferential direction, a "twisting" of the pipe as they propagate, while longitudinal and flexural modes induce particle motion both along the main axis of

National Energy Technology Laboratory (NETL) is the funding source for this effort with Cost Share being provided by Carnegie Mellon University (CMU). Concurrent Technologies Corporation (CTC) is funded under a cooperative agreement with NETL. CMU is funded under a Subcontract Agreement with CTC. N.O'Donoughue is supported by National Defense Science and Engineering Graduate Fellowship, sponsored by the Army Research Office.

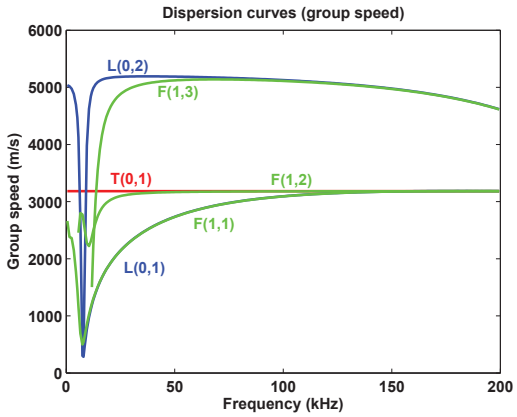


Fig. 1. Dispersion curve for the pipe modeled in our simulations, showing wavenumber vs. frequency for Longitudinal, Torsional, and first-order Flexural modes for f=0-50kHz.

the pipe and orthogonal to the surface of the pipe, and arise as an extension of the symmetric and anti-symmetric modes present in thin plates. Torsional and longitudinal modes are both axisymmetric, while flexural modes are not.

An important component of guided wave propagation is frequency dispersion [4], [8]. Each wave mode has its own dispersion curve, a representation of both the group velocity and phase velocity of that wave mode for various frequencies. See figure 1 for a plot of wavenumber ($k = 2\pi f/\nu(f)$, with propagation speed $\nu(f)$) vs. frequency. Some wave modes, like the second longitudinal mode (see L(0,2) in figure 1), have a region of relatively low dispersion (40-100kHz here). This encourages many system designers to limit the frequencies that they utilize. Other wave modes, like most of the flexural modes (see F(*,*) in figure 1), exhibit dispersion over most of their frequency range, although its effects are also most clear near the lower frequencies of support for each mode. The first torsional wave mode (see T(0,1) in figure 1), however, is unique in that it, alone among guided waves, does not experience dispersion. This is why many system designers choose to employ large arrays of transducers (on the order of 64 or 128), to selectively excite the first Torsional wave mode. Unfortunately, this mode is not always the most favorable in terms of propagation distance, thus we hope to excite all of the pipe's supported wave modes.

In lieu of a detailed analysis of each wave mode, for which the reader is referred to [8], we will simply consider the overall response of the system. This response is expressed as a function of the input frequency, and the transmitter and receiver locations: $H(\omega, \mathbf{x}_t, \mathbf{x}_r)$. In this paper, we make the assumption that the response is reciprocal. We consider a system with a single transmitter A, and an array of receivers B, placed around the pipe, some distance away. We assume that array B has N elements. The response of the system from transmitter A to the $i^{th}$ element of B is written

$$h_i(\omega) = H(\omega, \mathbf{x}_A, \mathbf{x}_{B_i}),\ i = 0, ..., N-1. \tag{1}$$

From this, we construct the frequency-dependent response matrix of dimension Nx1:

$$\mathbf{H}(\omega) = [h_0(\omega), h_1(\omega), ..., h_{N-1}]^T. \tag{2}$$

Furthermore, we assume that the background, or clutter, response of the system when there is no damage present is a stationary signal of the form $H_c(\omega)$, while the response of the system following damage is the superposition of $H_c(\omega)$ with a new set of waves induced by the damage:

$$H_{d+c}(\omega) = H_c(\omega) + H_d(\omega) \tag{3}$$

Finally, we make the assumption that, through repeated measurements, the clutter response $H_c(\omega)$ is known perfectly. For simplicity, we will refer to $H_d(\omega)$ as simply $H(\omega)$ for the remainder of this paper. It has been shown in [9], [10] that utilization of this damage response matrix in Time Reversal will result in coherent focused waves, under the presence of damage, and will result in white noise when the damage is absent. It is this principle that allows for Time Reversal detection of defects and damage.

### A. Data Model

Many of the following array definitions are taken directly from [10], and are repeated here merely to aid in the interpretation of our results. From (2), we can write the received signal for a snapshot at array B as

$$\mathbf{Y}_m(\omega) = \mathbf{H}(\omega)S(\omega) + \mathbf{V}_m(\omega) \tag{4}$$

Where the subscript $m$ refers to the snapshot number, and we have the complex white noise term $\mathbf{V}_m(\omega) \sim \mathcal{CN}\left(0, \sigma_v^2 \mathbf{I}_N\right)$. Next, we consider a band of frequencies $\{\omega_q\}_{q=0...Q-1}$ and define the column-stacked representation:

$$\begin{aligned}
\mathbf{Y}_m &= \left[\mathbf{Y}_m(\omega_0)^T, ...\mathbf{Y}_m(\omega_{Q-1})^T\right]^T \\
&= \mathbf{H}\mathbf{s}_A + \mathbf{v}_m && (5)\\
\mathbf{H} &= \text{diag}\left[\mathbf{H}(\omega_0), ...\mathbf{H}(\omega_{Q-1})\right]_{NQxQ} && (6)\\
\mathbf{s}_A &= \left[S(\omega_0), ...S(\omega_{Q-1})\right]^T && (7)\\
\mathbf{v}_m &= \left[\mathbf{V}_m(\omega_0)^T, ...\mathbf{V}_m(\omega_{Q-1})^T\right]^T && (8)
\end{aligned}$$

## III. Fault Detection

In this section, we will briefly lay out the detectors derived in [10]. We begin with the ideal (channel matched filter) detectors for both conventional and Time Reversal processing, for which the damage response $\mathbf{H}_d(\omega)$ is assumed to be known, and then describe the Generalized Likelihood Ratio Test detectors, for which a maximum likelihood estimate $\widehat{\mathbf{H}}_d(\omega)$ must be computed. First, however, we will describe the transmission schemes used to generate the data for detection.

### A. Time Reversal Transmission

We begin by transmitting $\mathbf{s}_A$ from antenna A into the damaged pipe, and remove the known clutter response.

$$\mathbf{Y}_m = \mathbf{H}\mathbf{s}_A + \mathbf{v}_m \tag{9}$$

This signal is then energy normalized, using the parameter:

$$k_m = \sqrt{\|\mathbf{s}_A\|^2 / \|\mathbf{Y}_m\|^2}. \quad (10)$$

The time-reversal probing signal to be sent from array B back to antenna A is given by:

$$\mathbf{s}_{TR} = k_m \mathbf{Y}_m^*. \quad (11)$$

Note that reversal of the time axis (for real-valued signals) is analogous to phase conjugation of the frequency content. The response after removal of the known clutter, at antenna A, to this input is given by:

$$X_m = k_m \mathbf{H}^T \mathbf{Y}_m^* + \mathbf{w}_m \quad (12)$$

$$= k_m \mathbf{H}^T \mathbf{H} \mathbf{s}_A^* + k_m \mathbf{H}^T \mathbf{v}_m^* + \mathbf{w}_m \quad (13)$$

where we have the white Gaussian noise term $\mathbf{w}_m \sim \mathcal{CN}\left(0, \sigma_w^2 \mathbf{I}_Q\right)$. Note the second term in the summation, which represents a retransmission of noise ($\mathbf{v}_m^*$) from the forward transmission.

### B. Conventional Transmission

For conventional detection, we will begin with the signal $S(\omega_q)$ transmitted from array B. Each element will transmit the same probing signal:

$$\mathbf{s}_B(\omega_q) = S(\omega_q)\mathbf{1}_{Nx1} \quad (14)$$

$$\mathbf{s}_B = \left[\mathbf{s}_B(\omega_0)^T, ..., \mathbf{s}_B(\omega_{Q-1})^T\right]^T \quad (15)$$

We define the energy normalization factor

$$\beta = \sqrt{1/N} \quad (16)$$

and transmit the scaled signal $\beta \mathbf{s}_B$. The received signal at A, following removal of the known clutter response, is:

$$\mathbf{r}_m = \beta \mathbf{H}^T \mathbf{s}_B + \mathbf{w}_m \quad (17)$$

### C. Channel Matched Filter

For the conventional case, the binary hypothesis test is:

$$\begin{array}{lll} \mathbb{H}_1 & : \mathbf{r}_m = & \beta \mathbf{H}^T \mathbf{s}_B + \mathbf{w}_m \\ \mathbb{H}_0 & : \mathbf{r}_m = & \mathbf{w}_m. \end{array} \quad (18)$$

Let $\mathbf{R} \triangleq \left[\mathbf{r}_0^T, ...\mathbf{r}_{M-1}^T\right]^T$ be the stacked snapshots of $\mathbf{r}_m$. From [10], it can be shown that this results in the CDCMF test statistic:

$$\ell_{CDCMF}(\mathbf{R}) = \Re\left\{ \frac{\left(\beta \mathbf{H}^T \mathbf{s}_B\right)^H \sum_{m=1}^M \mathbf{r}_m}{\sigma_w \left\|\beta \mathbf{H}^T \mathbf{s}_B\right\|} \right\}. \quad (19)$$

While, for Time Reversal, we have the binary hypothesis test:

$$\begin{array}{lll} \mathbb{H}_1 & : \mathbf{x}_m = & k_m \mathbf{H}^T \mathbf{H} \mathbf{s}_A + \mathbf{w}_m \\ \mathbb{H}_0 & : \mathbf{x}_m = & \mathbf{w}_m \end{array} \quad (20)$$

with $\mathbf{X}$ similarly defined. The TRCMF test statistic is given:

$$\ell_{TRCMF}(\mathbf{X}) = \Re\left\{ \frac{\left(\mathbf{H}^T \mathbf{H}^* \mathbf{s}_A^*\right)^H \sum_{m=1}^M \mathbf{x}_m}{\sigma_w \left\|\mathbf{H}^T \mathbf{H}^* \mathbf{s}_A^*\right\|} \right\}. \quad (21)$$

Note that, because the channel response is known fully, for the TRCMF, there is no retransmission of the noise term $\mathbf{v}_m$, as in (12).

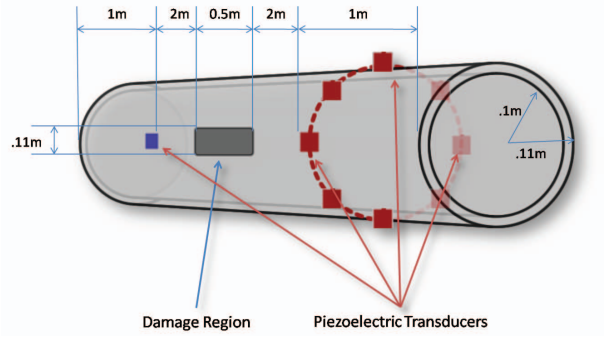


Fig. 2. Geometry of the pipe modeled.

### D. Generalized Likelihood Ratio Test

For the GLRT, it is assumed that both $\mathbf{Y}$ and $\mathbf{R}$ are available for conventional detection, and that both $\mathbf{Y}$ and $\mathbf{X}$ are available for Time Reversal detection. We refer the reader to [10] for a detailed derivation of the ML estimates $\widehat{\mathbf{H}}$ under both Time Reversal and conventional processing, as well as for the derivation of the GLRT detectors.

In the conventional case, we have the binary hypothesis test:

$$\begin{array}{lll} \mathbb{H}_1 & : \begin{bmatrix} \mathbf{y}_m \\ \mathbf{r}_m \end{bmatrix} = & \begin{bmatrix} \mathbf{H}\mathbf{s}_A \\ \beta \mathbf{H}^T \mathbf{s}_B \end{bmatrix} + \begin{bmatrix} \mathbf{v}_m \\ \mathbf{w}_m \end{bmatrix} \\ \mathbb{H}_0 & : \begin{bmatrix} \mathbf{y}_m \\ \mathbf{r}_m \end{bmatrix} = & \begin{bmatrix} \mathbf{v}_m \\ \mathbf{w}_m \end{bmatrix} \end{array} \quad (22)$$

which results in the CDGLRT test statistic:

$$\ell_{CDGLRT}(\mathbf{R}, \mathbf{Y}) = \frac{1}{\sigma_v^2 \sigma_w^2} \sum_{m=1}^M \left\{ 2\Re\left\{ \beta \sigma_v^2 \mathbf{s}_B^H \widehat{\mathbf{H}}^* \mathbf{r}_m + \sigma_w^2 \mathbf{y}_m^T \widehat{\mathbf{H}}^* \mathbf{s}_A^* \right\} - \sigma_w^2 \left\|\widehat{\mathbf{H}}\mathbf{s}_A\right\|^2 - \beta^2 \sigma_v^2 \left\|\widehat{\mathbf{H}}^T \mathbf{s}_B\right\|^2 \right\}. \quad (23)$$

For TR detection, we have the binary hypothesis test:

$$\begin{array}{lll} \mathbb{H}_1 & : \begin{bmatrix} \mathbf{y}_m^* \\ \mathbf{x}_m \end{bmatrix} = & \begin{bmatrix} \mathbf{H}^* \mathbf{s}_A^* \\ k_m \mathbf{H}^T \mathbf{H}^* \mathbf{s}_A^* \end{bmatrix} + \begin{bmatrix} \mathbf{v}_m^* \\ k_m \mathbf{H}^T \mathbf{v}_m^* + \mathbf{w}_m \end{bmatrix} \\ \mathbb{H}_0 & : \begin{bmatrix} \mathbf{y}_m^* \\ \mathbf{x}_m \end{bmatrix} = & \begin{bmatrix} \mathbf{v}_m^* \\ \mathbf{w}_m \end{bmatrix} \end{array} \quad (24)$$

and the TRGLRT test statistic:

$$\ell_{TRGLRT}(\mathbf{X}, \mathbf{Y}) = \frac{1}{\sigma_v^2 \sigma_w^2} \sum_{m=1}^M \left\{ 2\Re\left\{ k_m \sigma_v^2 \mathbf{y}_m^T \widehat{\mathbf{H}}^* \mathbf{x}_m + \sigma_w^2 \mathbf{y}_m^T \widehat{\mathbf{H}}^* \mathbf{s}_A^* \right\} - \sigma_w^2 \left\|\widehat{\mathbf{H}}\mathbf{s}_A\right\|^2 - k_m^2 \sigma_v^2 \left\|\widehat{\mathbf{H}}^T \mathbf{y}_m^*\right\|^2 \right\}. \quad (25)$$

## IV. Numerical Simulation

For numerical simulations, we use the commercial modeling software PZFlex. A sample pipe was generated, see figure 2 for the pipe dimensions and transducer layout. In this simulation, we consider corrosion on the interior surface of the pipe, modeled as a loss of wall thickness, while the transducers

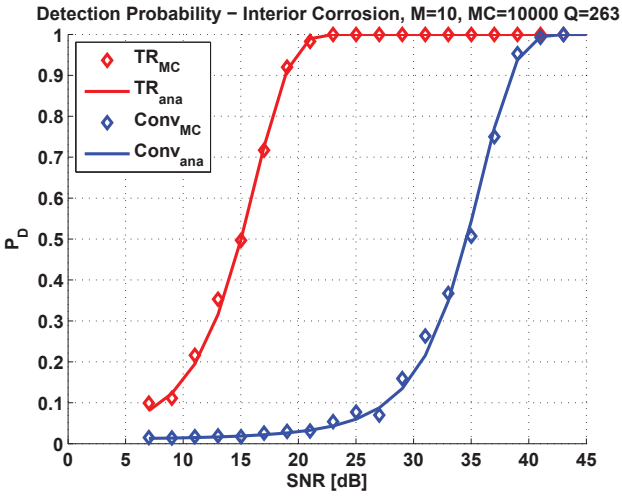


Fig. 3. Channel Matched Filter results show $P_D$ vs. SNR [dB] for both CDCMF(right) and TRCMF(left)

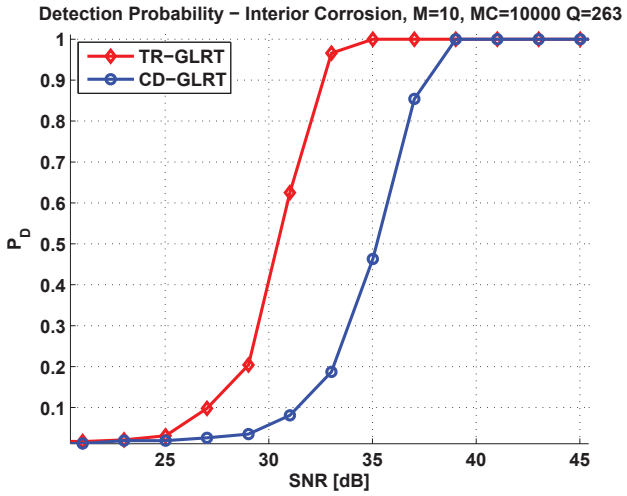


Fig. 4. Generalized Likelihood Ratio Test results show $P_D$ vs. SNR [dB] for both CDGLRT(right) and TRGLRT(left)

are attached to the outside of the pipe. The input pulse was a sinc with cutoff frequency $f_c = 200kHz$.

For detection, we generate random noise at various SNR levels, and run Monte Carlo simulations with 10,000 trials. For each trial, we take $M = 10$ snapshots, set $P_{FA} = 0.01$ and compute the analytical threshold according to (45) in [10]. The array B has $N = 8$ elements evenly spaced around the pipe. We used $Q = 263$ frequency samples, this number was computed from the coherence bandwidth with (74) in [10].

The results for the ideal channel matched filter are provided in figure 3. As can be seen from that image, Time Reversal can achieve comparable performance to conventional detection in the presence of an additional 20dB of noise. Although the 20dB improvement may seem extreme, it is corroborated by analytical predictions from (71) in [10] (reproduced below), which predicts 27.8dB for the data we provided.

$$SNRG_{max} = \frac{\|\mathbf{s}_A\|^2 \|\mathbf{H}^T \mathbf{H}^* \mathbf{s}_A^*\|^2}{\beta^2 \|\mathbf{H}^T \mathbf{s}_B\|^2 \|\mathbf{H}\mathbf{s}_A\|^2} \tag{26}$$

Moving to the GLRT case, we computed the threshold numerically using the data under $\mathbb{H}_0$ and $P_{FA} = 0.01$, and compared to the output of (23) and (25). The detection results are shown in figure 4. From these results, we can see a performance increase of 5dB. The difference between performance increase in the CMF and GLRT can be explained by 1) uncertainty and errors in the estimate of the channel response $\mathbf{H}$ and 2) the retransmission of noise terms, which causes some of the energy budget in the TR retransmission to be wasted on signal components that do not coherently focus.

## V. Conclusion

In this paper, we have shown the application of Time Reversal change detectors to acoustic guided waves propagating in a hollow pipe. We have demonstrated that the performance of such a system shows significant improvement, roughly 5dB with the GLRT, and shows the potential for as much as 30dB in the scenario described. Furthermore, we have shown that such results are possible by utilizing effects of dispersion, which allows broadband operation. This opens the possibility of improved resolution and efficiency, when compared to narrowband implementations. It remains to be shown what additional range this will impart on a Time Reversal based system, as well as what performance increase is seen over a pulse-echo design.

## References


[1] "PHMSA stakeholder communications: Pipeline incidents and mileage reports," U.S. Department of Transportation Pipeline and Hazardous Materials Safety Administration, Tech. Rep.

[2] J. J. Ditrai, "Utilization of guided elastic waves for the characterization," *J. Acoustic. Soc. Am.*, vol. 96, pp. 3769–3775, 1994.

[3] P. Cawley, "Practical long range guided wave inspection - managing complexity," in *29th Annual Review of Progress in Quantitative Nondestructive Evaluation*. American Institute of Physics, 2003, vol. 22, pp. 22–40.

[4] J. Li and J. L. Rose, "Excitation and propagation of non-axisymmetric guided waves in a hollow cylinder," *J. Acoust. Soc. Am.*, vol. 109, no. 2, pp. 457–464, February 2000.

[5] M. Fink, "Time Reversal of ultrasonic fields, I: Basic principles," *IEEE Trans. on Ultrasonics, Ferroelectrics, and Frequency Control*, vol. 39, pp. 555–566, 1992.

[6] R. K. Ing and M. Fink, "Time-reversed Lamb Waves," *IEEE Trans. on Ultrasonics, Ferroelectrics, and Frequency Control*, vol. 45, no. 4, pp. 1032–1043, 1998.

[7] C. Prada and M. Fink, "Separation of interfering acoustic scattered signals using the invariants of the time-reversal operator. application to lamb waves characterization." *J. Acoustic. Soc. Am.*, vol. 104, no. 1, pp. 801–807, 1998.

[8] N. O'Donoughue, J. Harley, J. M. F. Moura, Y. Jin, I. Oppenheim, Y. Ying, J. States, J. Garrett, and L. Soibelman, "Single-antenna time reversal of guided waves in pipes," *Proceedings of 158th Meetings on Acoustics*, April 2009.

[9] J. M. F. Moura and Y. Jin, "Detection by Time Reversal: Single antenna," *IEEE Trans. on Signal Processing*, vol. 55, no. 1, pp. 187–201, January 2007.

[10] Y. Jin and J. M. F. Moura, "Time-Reversal detection using antenna arrays," *IEEE Trans. on Signal Processing*, vol. 57, no. 4, pp. 1396–1414, April 2009.